Raman spectroscopic detection using a two-dimensional echelle spectrometer*

ZHANG Rui (张锐)**, **REN Wenyi** (任文艺), **WANG He** (王鹤), **WANG Yuanyuan** (王元元), **LIN Zhenkun** (林桢坤), **and HAN Ziqi** (韩孜琦)

School of Science, Northwest Agriculture and Forestry University, Yangling 712100, China

(Received 7 April 2021; Revised 25 May 2021)

In order to meet the high-resolution and wide spectrum range of the backscattering Raman system, this paper designs and builds a Raman test system based on the echelle spectrometer. In the optical splitting system, compared with the ordinary planar grating spectrometer, the use of the echelle improves the resolution of the system without increasing the volume of the system. The use of intensified charge-coupled device (ICCD) in the detection system improves the signal-to-noise ratio (*SNR*) and the detection limit of weak spectrum. Finally, the Raman system was spectrally calibrated. The broadband backscattering Raman experimental results are given and discussed. The experimental results show that the system has an excellent application prospect for broadband and high-resolution Raman spectrum measurement.

Document code: A **Article ID:** 1673-1905(2021)11-0641-5

DOI https://doi.org/10.1007/s11801-021-1065-7

In 1928, Raman spectrum was first discovered by Indian scientist Raman[1]. The Raman scattering spectra can fully reflect the structure and functional group information of the substance. The Raman scattering system has low requirements for sample preparation, which can be used to test various forms of samples (solid, gas, liquid)[2-4]. Moreover, it has the characteristics of remote, non-contact, non-destructive measurement, and has irreplaceable advantages in the detection of some dangerous substances and expensive substances[5]. Therefore, Raman spectroscopy is widely used in medical, chemical, industrial, environmental detection and other fields[6-9].

The Raman system is mainly composed of excitation system, optical splitting system, and receiving system[10,11]. Among them, the optical splitting system directly affects the resolution and spectral range of the entire system, which determines the fineness and comprehensiveness of element analysis[12]. Therefore, the urgent need for Raman measurement systems is mainly to study optical splitting system with high resolution and wide spectral detection range. In addition, due to the nature of Raman scattering light, the intensity of the Raman spectra is generally weak. However, the energy of the laser excitation source cannot be set too high, if it is set too high, it will cause thermal and photochemical damage to the sample. Therefore, the signal-to-noise ratio (*SNR*) measured by Raman system is generally low.

As a grating dispersive spectrometer, the echelle spectrometer mainly uses the echelle as the main dispersive element, which has the advantages of high resolution, high dispersion rate, high diffraction efficiency, full spectrum transient direct reading and so on[13-15]. Therefore, compared with the general planar grating spectrometer and concave grating spectrometer, the echelle spectrometer has a better balance between the band range and the spectral resolution. In addition, the use of intensified charge-coupled device (ICCD), which has refrigeration function, makes the whole spectrometer have high *SNR* and high sensitivity, which can well alleviate the problem of weak spectral signal intensity and low *SNR* of Raman system. In summary, it has certain advantages to use the echelle spectrometer as the optical splitting system of Raman system.

In view of this, this paper studies the backscattering Raman spectroscopy detection system based on the echelle spectrometer. First of all, according to the requirements of Raman spectroscopy for high resolution and broadband range, the optical splitting system with echelle grating as the main dispersive element was designed and developed. Then, according to the characteristics of the weak Raman intensity, the ICCD with better signal-to-noise performance is selected as the signal detector. The detector has high sensitivity to weak signal, which can improve the receiving ability of the whole

* This work has been supported by the Shaanxi Province Introduces Special Funds for Domestic Doctors (No.F2020221016), the Special Fund for Basic Scientific Research Business Expenses of Northwest Agriculture and Forestry University (No.Z1090321031), the National Natural Science Foundation of China (No.12004312), and the Innovation and Entrepreneurship Training Program of Shanxi Province (Nos.S202010712512 and S202110712187).

** E-mail: zhangrui_grating@163.com

system. In the process of Raman spectrum detection, the backscattering light path can be used to measure the Raman spectra of samples without light transmittance. Therefore, we choose the way of receiving backscattered light to study the Raman spectrum detection system based on the echelle grating spectrometer, and complete the spectral calibration of the whole system. Through experiments, a variety of samples were tested to complete the characteristic spectrum identification of the characteristic elements in the samples, and the detection of broadband backscattered Raman spectroscopy was realized.

The structure of the backscattering Raman spectrum detection system is shown in Fig.1.

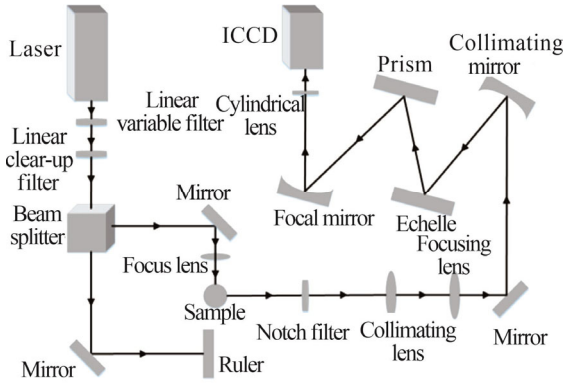

Fig.1 Structure of the backscattering Raman spectrum detection system

The Raman system is composed of three parts: excitation system, optical splitting system, and spectrum detection system. In the excitation system, the single wavelength laser (MSLFN-532, Changchun New Industries Optoelectronics Technology Co., Ltd.) with 532 nm wavelength is selected as the excitation source, and the tunable attenuator is placed at the back-end to make the laser energy adjustable in the range from 0 to 400 mW. After adjusting the intensity of light, the incident laser is purified by narrow-band filter, and then converged on the sample surface by the focusing system. The Raman spectra from the sample surface are collected in the optical splitting system by the focusing system after the Rayleigh scattering light is eliminated by the notch filter. The optical splitting system is mainly composed of the echelle grating and wedge prism. As the main dispersive element, the echelle has high resolution and high diffraction rate, which can ensure the resolution of the optical splitting system. As a cross-dispersion element, the prism eliminates the problem of spectral order overlap caused by the echelle. In order to make the spectra diffracted by echelle incident to the next optical element completely, the echelle is placed in the echelle spectrometer with a certain offset angle. The diffraction equation can be expressed as:

$$\frac{m\lambda}{\cos\varphi} = d(\sin\alpha + \sin\beta), \tag{1}$$

where d is the groove spacing, α is the incidence angle of the echelle, β is the diffraction angle of the echelle, φ is the grating offset angle, m is the grating diffraction order, and λ is the incident light wavelength.

In order to eliminate the serious spectral overlap after passing through the echelle, the wedge prism with the dispersion direction perpendicular to the dispersion direction of the echelle is placed at the back of the echelle. The refractive index of prism for different wavelengths is different. The overlapping spectral orders can be pulled perpendicular to the grating dispersion direction. Therefore, the main function of prism as a transverse dispersion element is to separate all levels of spectrum which are seriously overlapped after dispersion of echelle. Its dispersion capability has no effect on the resolution of the whole instrument. Therefore, the resolution of the optical splitting system is mainly determined by the resolving power of the echelle. When the echelle works under the condition of quasi littrow, the theoretical resolution is:

$$R = \frac{L(\sin\alpha + \sin\beta)\cos\varphi}{\lambda} = mN, \tag{2}$$

where L is the width of the grating, R is the theoretical resolution of the echelle, N is the total number of echelle, and m is the diffraction order. Therefore, the echelle working at high diffraction order and large diffraction angle can achieve high spectral resolution.

Finally, a two-dimensional spectrum is formed on the image surface after two dispersive elements are placed perpendicular to each other. Therefore, the spectral detection system uses two-dimensional array detector. Because of the weak signal intensity of Raman spectra, the *SNR* is low. In particular, ICCD (iKon-M 934, Andor) with refrigeration noise reduction and spectral signal enhancement function is selected as the receiver to improve the spectral reception efficiency.

Based on the backscattering Raman spectra system of the echelle spectrometer, the spectrum received by the spectrum detection system is a complex two-dimensional spectrum. From this spectrum, only the light intensity at the corresponding image plane position can be obtained, and the corresponding light wavelength at that position cannot be directly obtained. Therefore, it is necessary to establish a spectrum reduction model according to the transmission characteristics of light in each optical element, and determine corresponding wavelength value of each coordinate position of the image surface. Then, the obtained two-dimensional spectrogram is reduced to one-dimensional spectrogram which can reflect the relationship between wavelength and light intensity.

First, the echelle is assumed to be dispersive in Y direction. Prism is dispersive in X direction. Differential Eq.(1) can be used to calculate the angular dispersion of echelle.

$$\frac{\mathrm{d}\beta}{\mathrm{d}\lambda} = \frac{m}{d\cos\beta\cos\varphi}. \tag{3}$$

The wavelength range of each diffraction order of the echelle can be expressed as

$$\Delta\lambda = \frac{\lambda}{m}. \tag{4}$$

The dispersion angle of each wavelength can be calculated by combining Eq.(3) and Eq.(4) as

$$\gamma = \frac{\lambda}{d\cos\beta\cos\varphi}. \tag{5}$$

According to the dispersion angle of each wavelength and the structural parameters of the optical splitting system, the Y coordinate of each wavelength corresponding to the image plane can be obtained.

Similarly, according to the dispersion characteristics of the prism, the light passing through the prism satisfies

$$\varepsilon=\arcsin\{n(\lambda)\sin|2\delta-\sin^{-1}\theta/n(\lambda)|\}, \tag{6}$$

where ε is the exit angle of the prism, $n(\lambda)$ is the refractive index of the prism, δ is the apex angle of the prism, and θ is the incident angle of the prism. According to the prism exit angle, the dispersion angle of each wavelength in the prism dispersion direction can be uniquely determined, and then the X coordinate of each wavelength corresponding to the image plane can be determined.

Based on the above theoretical analysis, a spectral reduction model is established to determine the image plane position coordinates corresponding to different wavelengths of incident light. Furthermore, the relationship between the wavelength and the intensity of the incident light at different positions is obtained.

A standard mercury lamp with known wavelength was used to calibrate the Raman system. To reduce the interference of ambient light, turn off all other lighting sources. The wavelength calibration of the system is completed by adjusting the parameters of the model and matching the calculated results with the experimental results. Finally, the two-dimensional spectrum of the mercury lamp actually photographed by the system is shown in Fig.2(a), and the corresponding relationship between the wavelength of the incident light and the light intensity after calibration is shown in Fig.2(b).

After calibration, the system accurately recognizes the characteristic wavelengths of mercury lamps at 546.075 nm, 576.961 nm, 579.067 nm and so on.

The calibrated Raman system is used to test the solid samples and analyze whether the characteristic peaks of molecules in the samples can be accurately detected.

When the sample receives the laser energy, the laser interacts with the molecules in the sample. After the interaction, if the laser energy does not change, Rayleigh scattering will occur. If the molecule absorbs the laser energy, the molecule will be excited from the low energy state to the high energy state, the laser frequency will decrease, and Stokes scattering will occur. If the laser absorbs the molecular vibration and rotation energy, the molecule will jump from the high energy state to the low energy state, the laser frequency will increase, and anti-stokes scattering will occur. Anti-stokes scattering and Stokes scattering will be symmetrically distributed on both sides of Rayleigh scattering. However, there are more molecules in ground state and less in excited state. Therefore, we usually only focus on Stokes lines with higher energy. The characteristic line position of Raman spectra is generally expressed by the Raman displacement (wavenumber relative to the incident laser wavelength).

$$Raman\ shift = \frac{1}{\lambda_0} - \frac{1}{\lambda_i}, \tag{7}$$

where λ_0 is the wavelength of the incident laser light and λ_i is all the wavelengths in the spectral band of the spectrometer.

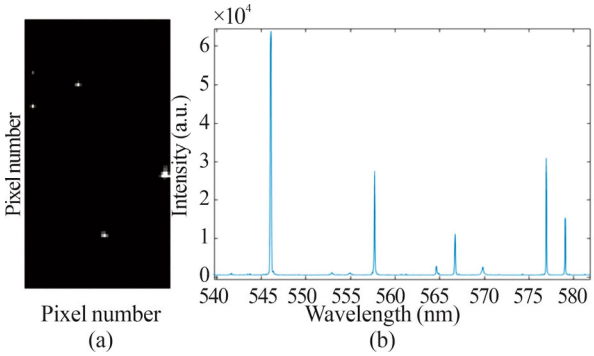

Fig.2 Schematic of mercury lamp spectrum: (a) Two-dimensional spectrum; (b) One-dimensional spectrum

The laser with 532 nm wavelength is used to irradiate the diamond sample, and the Raman spectrum of the diamond is shown in Fig.3. The first-order Raman characteristic peak of single crystal diamond is located at 1 332 cm^{-1}. At present, this peak has been recognized as the characteristic peak of diamond crystal derived from sp3 bond. The common impurity in diamond, sp2 non-diamond carbon, also has strong Raman activity. The D peak caused by its disorder and the G peak caused by the E_{2g} vibration mode are located near 1 350 cm^{-1} and 1 580 cm^{-1}, respectively. Among them, the ratio of the peak intensity of G peak to the peak intensity of diamond is also an important basis for evaluating the quality and purity of diamond. According to the systematic test results of this article, the diamonds used are of extremely high purity, and no D and G peaks caused by impurities are found.

Fig.4 shows the Raman spectra of sulfur powder in the range of 50—550 cm^{-1} at different integration times when the experimental laser power is constant. The characteristic peaks of sulfur at 84 cm^{-1}, 219 cm^{-1}, 247 cm^{-1}, 436 cm^{-1}, and 472 cm^{-1} were clearly detected. Among them, 219 cm^{-1} and 472 cm^{-1} have higher spectral intensity. This is because the elemental sulfur structure in the sulfur sample is a sawtooth ring structure composed of eight atoms in a closed ring. The characteristic peak at 219 cm^{-1} is generated by the bending vibration of the S_8

ring. The symmetric stretching vibration of the S_8 ring produces a characteristic peak at 472 cm^{-1}. The characteristic peak at 84 cm^{-1} is generated by other vibration modes of the S_8 ring. The integration time gradually changes from 0.01 s to 5 s. With the increase of integration time, the intensity of the feature spectrum detected by the system increases, which makes it easier to identify the feature peaks with relatively weak intensity.

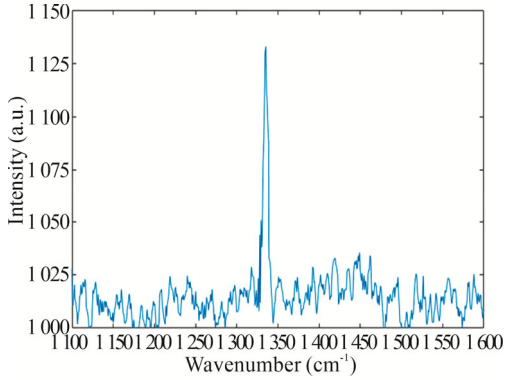

Fig.3 Raman spectrum of diamond

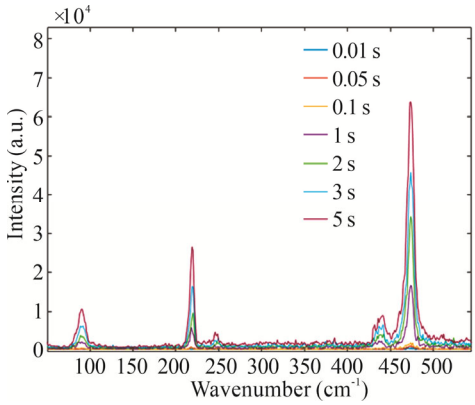

Fig.4 Raman spectra of sulfur at various integration times

The Raman spectra of potassium sulfate (K_2SO_4) were tested under different integration times. K_2SO_4 is an inorganic salt composed of sulfate ions and potassium ions. It is usually a colorless or white powder. It is often used in the preparation of fertilizers and glass. The Raman characteristic lines generated by different lattice vibration modes of potassium sulfate powder are shown in Fig.5. The free sulfate ion (SO_4^{2-}) has Td symmetry, and the characteristic lines generated by the internal vibration mode of the ion appear above 400 cm^{-1}. The characteristic spectrum of 449 cm^{-1} is generated by double degenerate vibration mode E (ν_2). The characteristic spectral line at the position of 619 cm^{-1} corresponds to the triple degenerate vibration mode F_2 (ν_4). The spectrum of fully symmetric vibration mode A_1 (ν_1) is located at 983 cm^{-1}.

Under the same conditions and different integration times, the characteristic peak of S-O symmetric stretching vibration in sodium sulfate (Na_2SO_4) is located at 993 cm^{-1}, which has good peak type and high intensity. It is often used to characterize the Raman characteristic peak of Na_2SO_4.

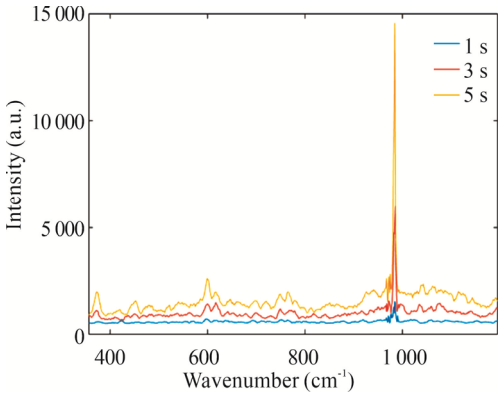

Fig.5 Raman spectra of K_2SO_4 at various integration times

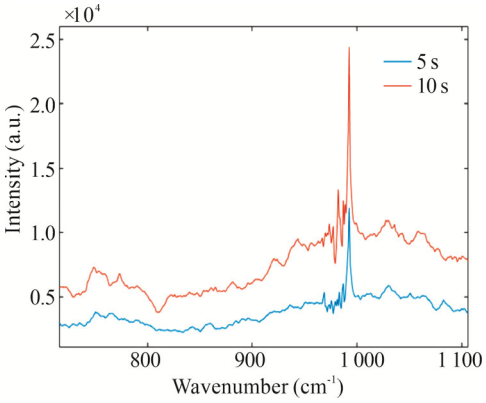

Fig.6 Raman spectra of Na_2SO_4 at various integration times

Mix the K_2SO_4 and Na_2SO_4 evenly in a mass ratio of 1:1. The characteristic peak position of K_2SO_4 differs from that of Na_2SO_4 by only 10 cm^{-1}. After testing, the characteristic spectral lines of the two samples can be clearly identified. Therefore, the Raman system based on the echelle spectrometer can identify the spectral lines with relatively close peak positions and clearly distinguish the different substances contained in the sample.

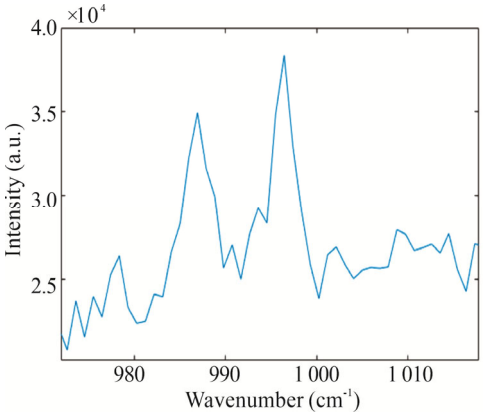

Fig.7 Raman spectrum of K_2SO_4 and Na_2SO_4 mixture with integration time of 10

The potassium carbonate (K_2CO_3) solid powder was also tested. The Raman characteristic peak of K_2CO_3 is generated by the free carbonate ion (CO_3^{2-}) at 1 058 cm^{-1}, which vibrates in a completely symmetrical way A_1 (ν_1).

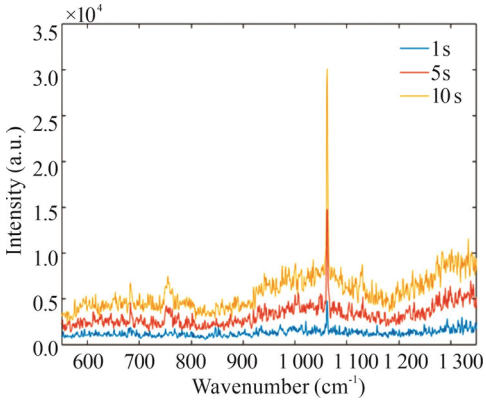

Fig.8 Raman spectra of K_2CO_3

K_2CO_3 and K_2SO_4 were evenly mixed at a mass ratio of 1:1, and the test was conducted under an integration time of 10 s. The characteristic peaks at 983 cm^{-1} and 1 058 cm^{-1} of the sample can be clearly identified.

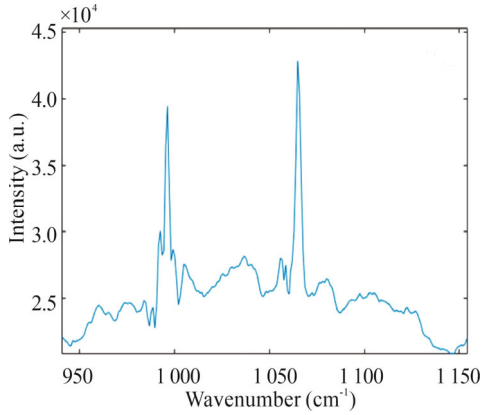

Fig.9 Raman spectrum of Na_2SO_4 and K_2CO_3 mixture with integration time of 10 s

Through the above experimental analysis, the backscattering Raman system based on the echelle spectrometer developed in this paper has successfully analysed the characteristic Raman spectrum lines of the characteristic elements contained in the sample. Without any moving parts, the calibration of the Raman system and the measurement of the Raman spectra are completed. The detection of different samples by Raman spectroscopy is realized. The backscattering Raman spectrum system based on the echelle spectrometer has the advantages of no moving parts and non-contact spectra detection, which is very suitable for the detection of dangerous explosives and industrial application fields.

References

[1] RAMAN C V, KRISHNAN K S. A new type of secondary radiation[J]. Nature, 1928, 121(3048): 501-502.

[2] QIN J K, LIAO P Y, SI M W, et al. Raman response and transport properties of tellurium atomic chains encapsulated in nanotubes[J]. Nature electronics, 2020, 3(3): 141-147.

[3] JAAFREH S, VALLER O, KREYENSCHMIDT J, et al. In vitro discrimination and classification of microbial flora of poultry using two dispersive Raman spectrometers (microscope and portable fiber-optic systems) in tandem with chemometric analysis[J]. Talanta, 2019, 202: 411-425.

[4] HOYOS L S, FAROLDI B, CORNAGLIA L. Reactivity of rice husk-derived lithium silicates followed by in situ Raman spectroscopy[J]. Journal of alloys and compounds, 2019, 778(25): 699-711.

[5] LIU J L, BAYANHESHIG, QI X D, et al. Backscattering Raman spectroscopy using multigrating spatial heterodyne Raman spectrometer[J]. Applied optics, 2018, 57(33): 9735-9745.

[6] QIU S F, LI M M, LIU J, et al. Study on the chemo-drug-induced effect in nasopharyngeal carcinoma cells using laser tweezer Raman spectroscopy[J]. Biomedical optics express, 2020, 11(4): 1819-1833.

[7] ALATTAR N, DAUD H, MAJMAIE R A, et al. Surface-enhanced Raman scattering for rapid hematopoietic stem cell differentiation analysis[J]. Applied optics, 2018, 57(22): E184-E189.

[8] AYMEN M, SAMI S, AHMED S, et al. Correlation between Raman spectroscopy and electrical conductivity of graphite/polyaniline composites reacted with hydrogen peroxide[J]. Journal of physics D: applied physics, 2013, 46(33): 335103.

[9] HEULER J, HE S, AMBARDAR S, et al. Point-of-care detection, characterization, and removal of chocolate bloom using a handheld Raman spectrometer[J]. Scientific reports, 2020, 10(1): 9833.

[10] HU G X, XIONG W, SHI H L, et al. Raman spectroscopic detection using a two dimensional spatial heterodyne spectrometer[J]. Optical engineering, 2015, 54(11): 114101.

[11] FOSTER M J, STOREY J, ZENTILE M A. Spatial heterodyne spectrometer for transmission Raman observations[J]. Optics express, 2017, 25(2): 1598-1604.

[12] QIU J, QI X D, LI X T, et al. Development of a spatial heterodyne Raman spectrometer with echelle-mirror structure[J]. Optics express, 2018, 26(9): 11994-12006.

[13] ZHANG R, BAYANHESHIG, YIN L, et al. Wavelength calibration model for prism-type echelle spectrometer by reversely solving prism's refractive index in real time[J]. Applied optics, 2016, 55(15): 4153-4158.

[14] YIN L, BAYANHESHIG, YANG J, et al. High-accuracy spectral reduction algorithm for the echelle spectrometer[J]. Applied optics, 2016, 55(13): 3574-3581.

[15] ZHANG R, BAYANHESHIG, LI X T, et al. Establishment and correction of an echelle cross-prism spectrogram reduction model[J]. Optics communications, 2017, 403: 401-407.